Current Control of a Voltage Source Inverter connected to the Grid via LCL Filter

A. Papavasiliou, S.A. Papathanassiou, S.N. Manias, G. Demetriadis
School of Electrical and Computer Engineering
National Technical University of Athens, Greece

***Abstract*-The utilization of inverters for the interconnection of distributed generators to the grid requires application of control systems capable of regulating the active and reactive output current, ensuring high power quality levels and achieving relative immunity to grid perturbations. This paper proposes a simple current control scheme, based on the combination of deadbeat and PI control, for a three-phase voltage source inverter connected to the grid via an LCL filter. The control system is analyzed in the frequency domain and an analytical expression for the harmonic content of the output current is derived. Theoretical analysis and computer simulation results validate the stability, fast transient response and robustness of the proposed system to network disturbances, variations in filter parameters and measurement errors.**

***Keywords*-DC/AC inverters, current control, LCL filter, PI control, deadbeat control, dq transformation.**

I. INTRODUCTION

Power electronic converters are being increasingly utilized in distributed generation (DG) applications for the interconnection to the grid of the primary energy source, be it a PV array, a small wind turbine, a microturbine, a fuel cell etc. Converters utilized are typically one- or three- phase voltage source inverters, depending on the size of the source, connected to the grid via a filter, which in principle acts as a low-pass impedance attenuating the high frequency switching harmonics of the inverter.

Recently, LCL filters are gaining momentum as an attractive alternative to the simple series inductance output filters in high power quality applications. An important advantage of LCL filters is their capability of attenuating harmonics at lower frequencies, which is a significant feature for high power applications, and also their capacity for precise control of the output current. However, control systems involving LCL filters are inevitably more complicated and attention is required in their design for operation under distorted terminal voltage conditions.

Available literature concerning the control systems of LCL filtered inverters focuses on variations of the deadbeat predictive control and the PI control. Proposed strategies vary with respect to the target of control and the structure of the inner and outer loops. Simple strategies focus on the direct control of a single variable, such as the output or inverter current (respectively at grid- or inverter-side of the filter) [1]. A common approach comprises an outer control loop for capacitor voltage control [2] and an inner control loop for the inverter current. The drawback of this strategy is that the output current may be sensitive to grid perturbations, because it is not directly controlled. Another proposition is the implementation of an inner control loop for the capacitor voltage, which supports the control loop of the output current [3]. More complicated multivariable control techniques have also been proposed [4].

This paper proposes a novel and effective control strategy for DC/AC voltage source converters, connected to the grid via LCL filters. Compared to other controllers of the literature, the structure of the proposed control system, shown in Fig. 1, is rather intuitive, simple and straightforward. The output current is regulated via a PI controller whose output determines the current reference for an inner-loop deadbeat controller. Thus, the overall control is decomposed into two cascaded parts, facilitating the application of control analysis techniques for the design of a robust and well-damped control system. The proposed system is analyzed with respect to its transient response and its stability. The harmonic performance of the system is also evaluated, with emphasis on its harmonic impedance, as viewed from its output terminals, extending the results of previous work on the subject [5]. Time-domain simulation results are presented, in order to validate the theoretical analysis of the control system.

II. CONTROL STRATEGY

Fig. 1 explains the structure of the control system, which includes an external PI control loop for the output current regulation, stabilized by an inner loop deadbeat controller for the inverter current. The goal of the control scheme is to regulate the output current by appropriately modulating the PWM inverter. This is achieved in two stages: the output current i_{L_2} error is fed to a PI controller, which generates the reference value $i_{L_1}^*$ for the inverter current. The PWM inverter is then modulated according to the output of the inner deadbeat controller.

In Fig. 1, $Z_s=R_s+jL_s$ is the grid impedance, corresponding to a short circuit capacity S_k. For the derivation of transfer functions in the following, this impedance is incorporated in the impedance L_2 of the filter, yielding $L=L_2+L_s$, $R=R_s$. The inverter is assumed to have a nominal capacity of 100 kVA.

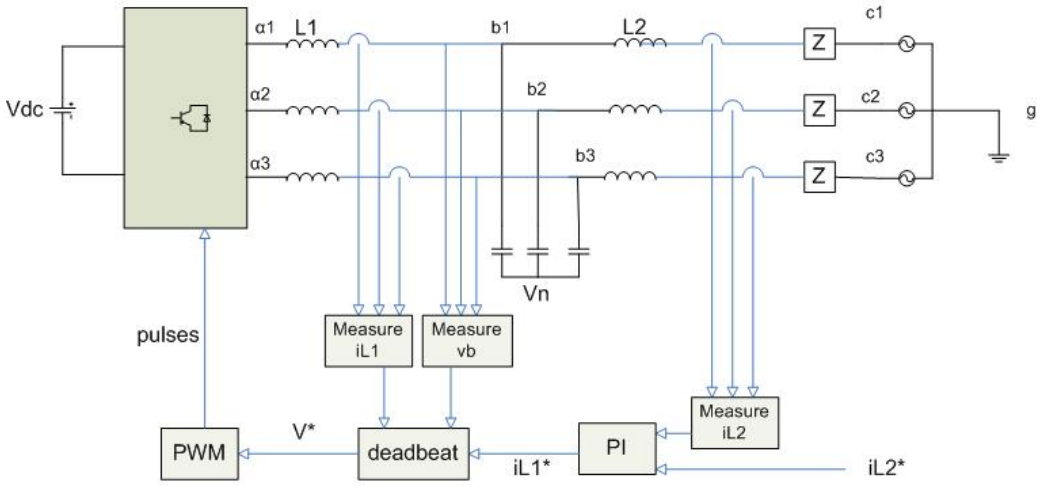

Figure 1: Simplified block diagram of the system, including the controllers.

In the analysis presented in the following, the dc voltage input to the inverter is assumed to be constant, which is an acceptable approximation when a reasonably large capacitor is connected at the inverter input. The output voltage of the modulator is modeled as a constant dc voltage per modulation period T_s (100 μs) equal to the average value of the input dc voltage. The sampling period for the deadbeat control is equal to T_s. Both the deadbeat and PI controllers are analyzed in the synchronous dq frame, which significantly simplifies controller design and stability analysis.

A. Deadbeat and PI Controllers

The deadbeat controller is presented in Fig. 2. For a sufficiently short PWM carrier period, T_s, it is possible to calculate the transfer function of the deadbeat controller with difference equations in the z-plane. Application of the z-transform implies that the capacitor voltage is considered constant throughout T_s, which is valid for sufficiently high switching frequencies. The controller is quite simple in principle. Feedback of i_{L1} is amplified by L_1/T_s and added to the measured capacitor voltage v_b, thus yielding the voltage signal V^* which is fed to the modulator. Given that v_b remains constant over T_s, the transfer function of the above system is given by eq. (1).

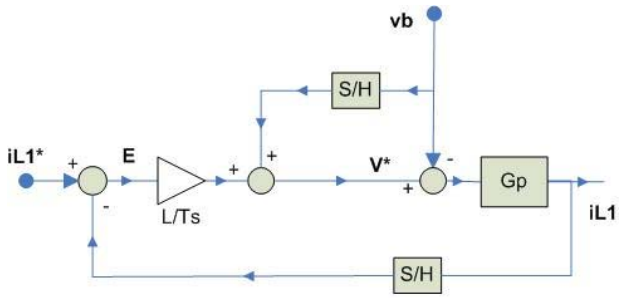

Figure 2: Control diagram for i_{L1}. The diagram refers to d and q axis components.

$$\mathbf{I}_{L_1}(z) = \left(\mathbf{I} + \mathbf{G}_p(z)\frac{L_1}{T_s}\right)^{-1} \mathbf{G}_p(z)\frac{L_1}{T_s}\mathbf{I}_{L_1}{}^*(z) \quad (1)$$

where the transfer function $\mathbf{G}_p(z)=V_{ab}(z)/I_{L1}(z)$[1] of L_1 is given by equation (2):

$$\mathbf{G}_p(z) = \frac{\begin{pmatrix}(z-1)\sin(\omega T_s) & (z+1)(1-\cos(\omega T_s))\\ (z+1)(\cos(\omega T_s)-1) & (z-1)\sin(\omega T_s)\end{pmatrix}}{\omega L_1(z^2 - 2z\cos(\omega T_s)+1)} \quad (2)$$

Assuming a sufficiently small T_s, $\mathbf{G}_p(z)$ in eq. (2) is simplified and substituted in eq. (1) yields:

$$\mathbf{I}_{L_1}(z) = \begin{pmatrix}\frac{1}{z} & 0\\ 0 & \frac{1}{z}\end{pmatrix}\mathbf{I}_{L_1}{}^*(z) \quad (3)$$

The structure of the external PI control loop is presented in Fig. 3. For the analysis in the following, the assumption is made that the output of the PI control is actually i_{L1}, not i_{L1}^*, because, as shown in eq. (3), i_{L1} follows i_{L1}^* with a lag of T_s, which is sufficiently small to ignore. The system is s-transformed on the dq frame. The transfer function of the PI controller is then given by eq. (4), i.e. the d and q axis currents are controlled via independent regulators.

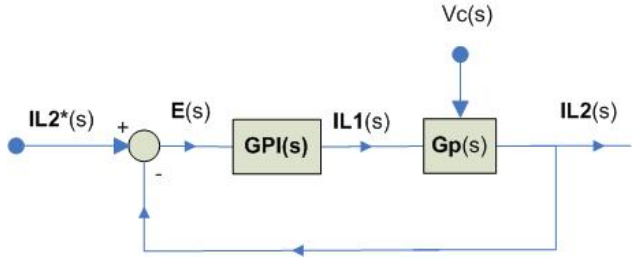

Figure 3: PI control of i_{L_2}. The diagram refers to d and q axis components.

[1]Symbols in bold denote vectors transformed in the synchronous dq frame.

$$\mathbf{G}_{PI}(s)=\begin{pmatrix} K_{p,d}+\dfrac{K_{i,d}}{s} & 0 \\ 0 & K_{p,d}+\dfrac{K_{i,d}}{s} \end{pmatrix} \tag{4}$$

$\boldsymbol{G}_p(s)=V_a(s)/I_{L_2}(s)$[2] is the transfer function of the network formed by C, L_2 and the grid impedance (see Fig. 1). The state equations of this subnetwork are given by eq. (5), where ω is the frequency of the synchronous dq frame, ($100\pi\ rs^{-1}$ for a 50 Hz network):

$$\frac{d}{dt}\mathbf{x}=\begin{pmatrix} -\dfrac{R}{L} & \omega & \dfrac{1}{L} & 0 \\ -\omega & -\dfrac{R}{L} & 0 & \dfrac{1}{L} \\ -\dfrac{1}{C} & 0 & 0 & \omega \\ 0 & -\dfrac{1}{C} & -\omega & 0 \end{pmatrix}\mathbf{x}+\begin{pmatrix} 0 & 0 & -\dfrac{1}{L} & 0 \\ 0 & 0 & 0 & -\dfrac{1}{L} \\ \dfrac{1}{C} & 0 & 0 & 0 \\ 0 & \dfrac{1}{C} & 0 & 0 \end{pmatrix}\mathbf{u} \tag{5}$$

$$\mathbf{y}=\begin{pmatrix} 1 & 0 & 0 & 0 \\ 0 & 1 & 0 & 0 \end{pmatrix}\mathbf{x}$$

$$\mathbf{x}=(i_{L_2d} \quad i_{L_2q} \quad v_{bd} \quad v_{bq})^T$$

$$\mathbf{u}=(i_{L_1d} \quad i_{L_1q} \quad v_{cd} \quad v_{cq})^T$$

Omitting the laborious algebra, an accurate approximation of the transfer functions of the PI controller on the synchronous dq frame is eventually given by eqs. (6).

$$\begin{pmatrix} I_{L_2d} \\ I_{L_2q} \end{pmatrix}=\begin{pmatrix} g_{11}(s) & g_{12}(s) & g_{13}(s) & g_{14}(s) \\ g_{21}(s) & g_{22}(s) & g_{23}(s) & g_{24}(s) \end{pmatrix}\begin{pmatrix} I_{L_1d} \\ I_{L_1q} \\ V_{cd} \\ V_{cq} \end{pmatrix} \tag{6}$$

$$g_{11}(s)=g_{22}(s)=\frac{-s^2bc+sabc+(c\omega^2b+c^2b^2)}{D(s)}$$

$$g_{12}(s)=-g_{21}(s)=\frac{s(-2\omega bc)+\omega abc}{D(s)} \tag{7}$$

$$g_{13}(s)=g_{24}(s)=\frac{s^3(-b)+s^2ab+s(cb^2-\omega^2b)+a\omega^2b}{D(s)}$$

$$g_{14}(s)=-g_{23}(s)=\frac{s^2(-\omega b)+(-\omega cb^2-\omega^3b)}{D(s)}$$

$$D(s)=s^4-2as^3+s^2(a^2+2\omega^2-2bc)+s(-2a\omega^2+2abc) \tag{8}$$
$$+(\omega^2(a^2+\omega^2)+(bc)^2+2bc\omega^2)$$

where D(s) is the characteristic polynomial of the transfer functions and a=-R/L, b=$1/L$, c=$1/C$. The PI controller ensures zero steady state error for the output current.

B. Stability Analysis

Since no specific value can be used for the Thevenin impedance of the network, L_2 is not used as a design parameter, in order to achieve robustness of the control scheme to grid impedance variations. Large values of C were observed to increase settling time, in addition to increasing the current through the capacitance and therefore the inverter switches. On the other hand, a combination of increased proportional gain and low capacitance causes overshoot and increased settling time. Large proportional gains cause large current overshoot without improving settling time, whereas variations in K_p, below a certain threshold, do not affect the system response. The integral gain was the most significant control parameter, and the locus in Fig. 4 is therefore drawn with respect to variations in K_i. Due to the presence of zeros in the neighborhood of the complex poles, the transient response of the system is dominated by the negative real pole. Hence, large values of integral gain significantly improve transient behavior, at the expense however of increased overshoot, due to the ineffective cancellation of the complex pairs of zeros and poles. Filter and control parameters were therefore chosen as a trade-off between speed of response and sufficient damping, i.e. stability margin: C=50 μF, L_2=10 μH, K_p=$4\cdot10^{-4}$, K_i=200. In order to determine a value for L_1, the system was design to resonate at f_{res}=1850 Hz in a grid with S_k=$20S_N$ (where S_N=100kVA is the rated inverter capacity).

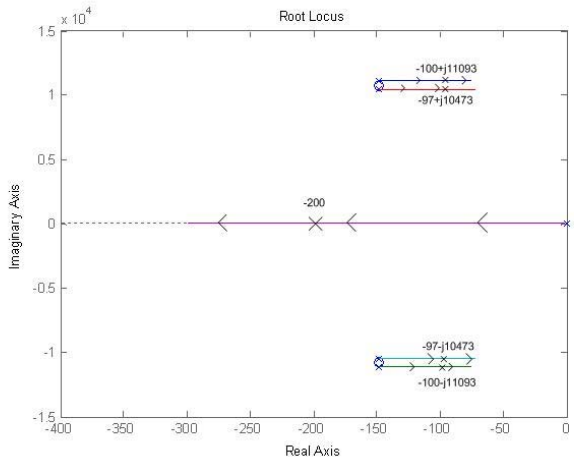

Figure 4: Root locus for $S_k = 20S_N$, $S_N = 100kVA$.

L_1 was chosen so as to achieve a resonance frequency of 8.15 kHz for the LCL filter. This is a desirable frequency because of its distance from the switching frequency, resulting in significant attenuation of switching harmonics. Assuming a symmetric network, the circuit of Fig. 1 can be analyzed per phase and the following transfer equation is obtained for the output current i_{L_2} with respect to network voltage:

$$\frac{I_{L_2}}{V_a}=\frac{1}{R+s(L_1+L_2)+s^2RL_1C+s^3L_1LC} \tag{9}$$

The above transfer function is analyzed in the frequency domain to obtain the resonance frequency. The first order conditions are given by the following equation:

$$\frac{d}{d\omega}\frac{1}{\sqrt{(R-\omega^2RL_1C)^2+(\omega(L_1+L)-\omega^3L_1LC)^2}}=0 \tag{10}$$

$$\Rightarrow AL_1^2+BL_1+C=0$$

where

[2] Under symmetric conditions, it can be shown that $v_n=v_g$. Hence, the notation $V_a(s)=V_{an}(s)=V_{ag}(s)$ is adopted.

$$A = 6\omega_{res}^5 (LC)^2 + 4\omega_{res}^3 (RC)^2 - 8\omega_{res}^3 LC + 2\omega_{res}$$
$$B = -8\omega_{res}^3 L^2 C + 4\omega_{res} L - 4\omega_{res} R^2 C \quad (11)$$
$$C = 2L^2 \omega_{res}$$

Solving the above quadratic equation with respect to L_1 for a resonance frequency of f_{res}=8.15 kHz, it is obtained L_1=1.1 mH.

III. Harmonic Impedance

In this section the effect of grid voltage distortion on the output current is investigated, by assuming the presence of specific harmonics at the terminal voltage. The goal is first to transform eqs. (6) to the natural phase coordinates (denoted *123*) in order to identify the effect of design parameters in the attenuation of harmonics of the output current, induced by the distortion of grid voltage.

The harmonic impedance of the system, as seen from the inverter terminals, is given by eq. (12), (its derivation is given in the Appendix):

$$\begin{pmatrix} I_{L_2 1}(s) \\ I_{L_2 2}(s) \\ I_{L_2 3}(s) \end{pmatrix} = \left(g_a(jn\omega - j\omega) + jg_b(jn\omega - j\omega)\right) \begin{pmatrix} V_{c1}(s) \\ V_{c2}(s) \\ V_{c3}(s) \end{pmatrix} \quad (12)$$

where n is the order of harmonic distortion, $\omega=2\pi f=100\pi$ is the angular speed of the rotating dq system, and

$$g_a(s) = \frac{A_3(s)}{P(s)} g_b(s) = \frac{A_4(s)}{P(s)} \quad (13)$$

In eq. (13), A_3(s), A_4(s) and P(s) are expressed in terms of the numerators N_{ij} of the polynomials g_{ij} appearing in eqs. (7):

$$A_3(s) = sN_{13}(sD + N_{11}(sK_p + K_i)) + sN_{14}N_{12}(sK_p + K_i)$$
$$A_4(s) = sN_{14}(sD + N_{22}(sK_p + K_i)) - sN_{13}N_{12}(sK_p + K_i) \quad (14)$$
$$P(s) = (sD + (sK_p + K_i)N_{11})^2 + N_{12}{}^2(sK_p + K_i)^2$$

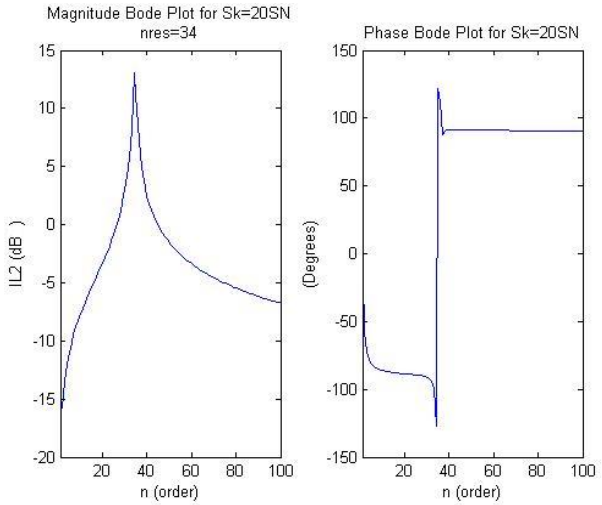

Figure 5: Bode diagram of transfer function $I_{L_2}(s)/V_c(s)$ ($S_k=20S_N$).

In Fig. 5 the Bode diagram of the transfer function is shown. Apparently, the system is capable of effectively attenuating low frequency harmonic distortion, inevitably present in the terminal voltage, which will not affect the output current significantly. The resonance has been tuned at relatively high frequencies (34th harmonic), that is well beyond the usual grid voltage distortion range, to ensure trouble-free operation of the system.

IV. Simulation Results

In the following, results are presented from the simulation of the inverter, using Matlab-Simulink. In Fig. 6 the response is shown to a step increase of the output current reference $i_{L_1}{}^*$. The response time is clearly shorter than one cycle (20 ms), while the steady state error is zero, confirming the good performance of the current controllers.

Control analysis and time-domain simulation results also confirm that the stability and transient behavior of the system are not affected by grid impedance variations, verifying thus the robustness of the control to changing grid conditions.

The important issue of the harmonic performance of the inverter is outlined in Figs. 7 and 8. In Fig. 7 the harmonic spectrum of the output current is shown, for operation of the inverter at rated power and terminal voltage conditions. First it is observed that the LCL filter effectively attenuates all switching frequency harmonic components (around 10 kHz and its multiples). The overall THD value of 1,6% is satisfactory and it is related to the spectral content around the 34th harmonic order. This is due to the under-damped transient oscillations, associated with the mode evident in the resonance of the Bode diagram of Fig. 5.

The other important consideration regarding the harmonic performance of the system is its behavior in case of distorted grid voltage conditions, as discussed in Section III. Fig. 8 shows the low order harmonics of the output current when the inverter is connected to a polluted grid, whose voltage comprises harmonics of the 5th, 7th and 11th order, respectively equal to 5.2%, 4.1% and 3% of the fundamental [6]. Now the output current inevitably exhibits increased low frequency distortion. However, the magnitude of the individual harmonics is low and the overall THD value is absolutely acceptable.

The system was also tested for robustness with respect to parameter values. In order to observe the effect of errors of parameter values in stability and control precision, we introduce a 15% error between the estimated and the actual value of L_1 and C with $L_{1r}=1.15L_1=1.625$ *mH*, where L_{1r} is the true value of the inductance and L_1 is the value used in the control system. The transfer function of the deadbeat controller now becomes:

$$\mathbf{I}_{L_1}(z) = \begin{pmatrix} (z-1+\frac{L_1}{L_{1r}})^{-1} & 0 \\ 0 & (z-1+\frac{L_1}{L_{1r}})^{-1} \end{pmatrix}^{-1} \frac{L_1}{L_{1r}} \mathbf{I}_{L_1}{}^*(z) \quad (15)$$

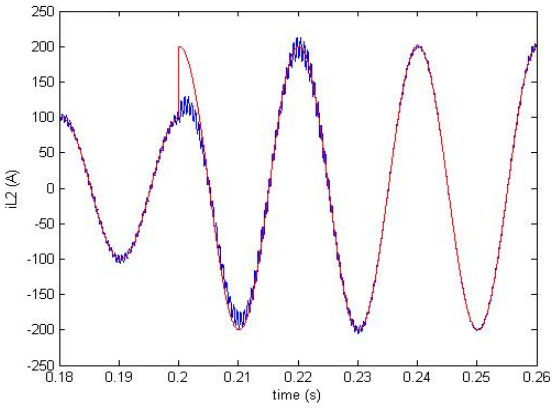

Figure 6: Step response of output current i_{L_2} (S_k=20S_N).

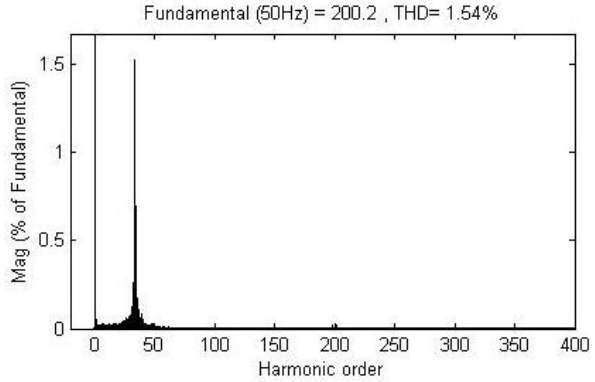

Figure 7: Harmonic spectrum of output current I_{L_2} ($S_k = 20S_N$).

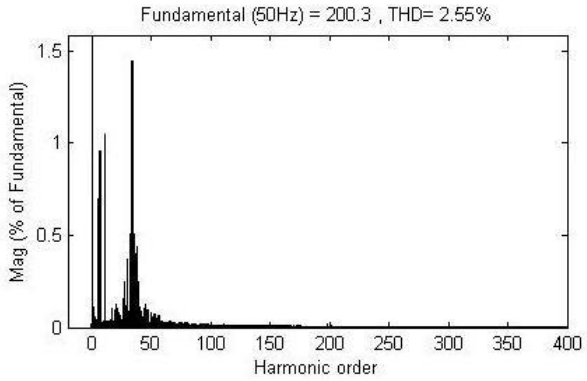

Figure 8: Harmonic spectrum of output current I_{L_2}, when the inverter operates under distorted grid voltage conditions ($S_k = 20S_N$).

Transforming eq. (15) in the time domain yields:

$$\mathbf{i}_{L_1}((k+1)T_s) - (1 - \frac{L_1}{L_{1r}})\mathbf{i}_{L_1}(kT_s) = \frac{L_1}{L_{1r}}\mathbf{i}_{L_1}^{*}(kT_s) \qquad (16)$$

The output of the deadbeat controller is not exactly equal to the control signal, but depends on the relative error of L_1 and the former value of i_{L_1}. However, the switching period is much smaller than L_1/L_{1r}, so the output of the deadbeat controller remains unaffected, with a very good approximation. Thus, due to the high switching frequency employed in the system, the effect of the error in the stability and precision of the control is negligible. This is evident in Fig. 9, where the transient response is plotted with and without error in L_1.

A similar test was conducted for an actual value of the capacitance C_{1r}=1.15C_1=75 μF. The accuracy of the control is not affected by this error since C does not enter as a parameter in the control loops. However, the roots of the transfer functions are shifted. The new poles, calculated from eq. (9), are given in Table 1. The system remains stable and simulation confirms the theoretical results.

Finally, the system was checked for robustness with respect to the characteristics of the grid. The poles of the system, calculated for a weaker grid (S_k=10S_N), are presented in Table 2. The results confirm that the stability properties remain unaffected, although the transient response presents now a differentiation in the frequencies and damping of the oscillations.

TABLE I
POLE POSITIONS WITH AND WITHOUT C VALUE ERROR

Without error	With error
-51±j11099	-52±j9119
-148±j11096	-148±j9117
-45±j10470	-45±j8491
-148±j10468	-148±j8489
-200±j0.06	-200±j0.1

TABLE II
POLE POSITIONS IN CASE OF WEAK GRID (S_K=10S_N)

-57±j8052
-153±j8051
-49±j7424
-153±j7423
-200±j0.1

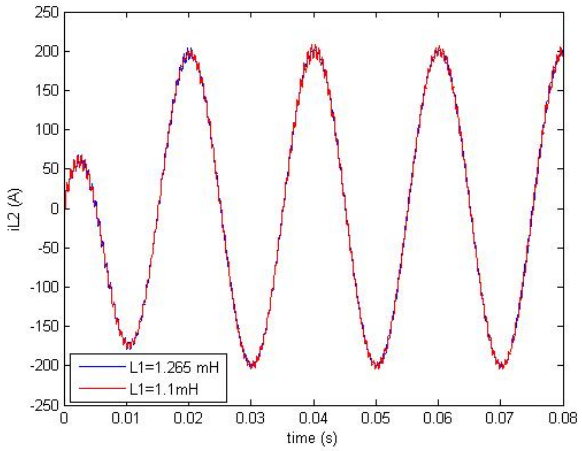

Figure 9: Transient response for L_{1r}=1.1mH (no error) and L_{1r}=1.265 mH (with error).

V. CONCLUSIONS

This paper proposes a control strategy for a voltage source inverter with an LCL output filter, suitable for interfacing dc voltage sources to the grid. The proposed control system is simple, exhibits satisfactory transient response and robustness to grid impedance variations. The linearized equations of the system are used to derive transfer functions, in order to select controller parameters and analyze its small signal stability. Its response characteristics are verified via time-domain simulation. The effectiveness of the LCL filter in attenuating the output current distortion is demonstrated and the important issue of the input harmonic impedance of the system is analyzed, verifying the immunity of the proposed controller to grid voltage distortion.

VI. APPENDIX: DERIVATION OF EQ. (12)

In the following, the notation $\omega=2\pi f=100\pi$ r/s is used for the angular velocity of the rotating dq axis. First, eqs. (7) are transformed to the stationary frame. The identities $cos(a)=(e^{ja}+e^{-ja})/2$, $sin(a)=(e^{ja}-e^{-ja})/2j$, as well as the Laplace transform property $L\{e^{j\omega t}f(t)\}=F(s-j\omega)$ are applied in the inverse Park transformation of i_{L2} to obtain the following equation:

$$\begin{pmatrix} I_{L_21}(s) \\ I_{L_22}(s) \\ I_{L_23}(s) \end{pmatrix} = \begin{pmatrix} \frac{I_{L_2d}(s-j\omega)+I_{L_2d}(s+j\omega)+jI_{L_2q}(s-j\omega)-jI_{L_2q}(s+j\omega)}{2} \\ \frac{e^{-j\frac{2\pi}{3}}I_{L_2d}(s-j\omega)+e^{j\frac{2\pi}{3}}I_{L_2d}(s+j\omega)+je^{-j\frac{2\pi}{3}}I_{L_2q}(s-j\omega)-je^{j\frac{2\pi}{3}}I_{L_2q}(s+j\omega)}{2} \\ \frac{e^{j\frac{2\pi}{3}}I_{L_2d}(s-j\omega)+e^{-j\frac{2\pi}{3}}I_{L_2d}(s+j\omega)+je^{j\frac{2\pi}{3}}I_{L_2q}(s-j\omega)-je^{-j\frac{2\pi}{3}}I_{L_2q}(s+j\omega)}{2} \end{pmatrix} \quad \text{(A1)}$$

A similar expression can be obtained for V_c. Next, combining eqs. (6) with eqs. (A1) and the corresponding expressions for the voltage, it is eventually obtained:

$$\begin{pmatrix} I_{L_21}(s) \\ I_{L_22}(s) \\ I_{L_23}(s) \end{pmatrix} = (g_{a,r}-g_{b,i}) \begin{pmatrix} V_{C1}(s) \\ V_{C2}(s) \\ V_{C3}(s) \end{pmatrix} + (g_{a,r}+g_{b,i}) \begin{pmatrix} \frac{-jV_{Cd}(s-j\omega)+jV_{Cd}(s+j\omega)+V_{Cq}(s-j\omega)+V_{Cq}(s+j\omega)}{2} \\ \frac{-je^{-j\frac{2\pi}{3}}V_{Cd}(s-j\omega)+je^{j\frac{2\pi}{3}}V_{Cd}(s+j\omega)+e^{-j\frac{2\pi}{3}}V_{Cq}(s-j\omega)+e^{j\frac{2\pi}{3}}V_{Cq}(s+j\omega)}{2} \\ \frac{-je^{j\frac{2\pi}{3}}V_{Cd}(s-j\omega)+je^{-j\frac{2\pi}{3}}V_{Cd}(s+j\omega)+e^{j\frac{2\pi}{3}}V_{Cq}(s-j\omega)+e^{-j\frac{2\pi}{3}}V_{Cq}(s+j\omega)}{2} \end{pmatrix} \quad \text{(A2)}$$

where $g_{a,r}$, $g_{a,i}$ are the real and imaginary parts respectively of $g_a(s)$ defined in eq. (13) (similarly for $g_{b,r}$, $g_{b,i}$). There still remains to express the second term of the right hand side of eqs. (A2) (denoted V_c' in the following) as a function of V_c. Considering a grid voltage harmonic component which is of order n and symmetric, its dq transformation to the synchronous frame, rotating at angular speed ω, will be:

$$\begin{pmatrix} V_{cd}(s) \\ V_{cq}(s) \end{pmatrix} = \hat{V}_c \begin{pmatrix} \cos\varphi\frac{s}{s^2+(n-1)^2\omega^2}-\sin\varphi\frac{(n-1)\omega}{s^2+(n-1)^2\omega^2} \\ \cos\varphi\frac{(n-1)\omega}{s^2+(n-1)^2\omega^2}+\sin\varphi\frac{s}{s^2+(n-1)^2\omega^2} \end{pmatrix} \quad \text{(A3)}$$

where φ is the angle of phase 1 with respect to the rotating frame at time 0 and $\hat{V}_c$ is the amplitude of the considered harmonic. Substituting eq. (A3) to eq. (A2) and omitting the algebra, it is finally obtained:

$$\begin{pmatrix} V'_{C1}(s) \\ V'_{C2}(s) \\ V'_{C3}(s) \end{pmatrix} = \hat{V}_c \begin{pmatrix} \cos\varphi\frac{n\omega}{s^2+n^2\omega^2}+\sin\varphi\frac{s}{s^2+n^2\omega^2} \\ \cos(\varphi-\frac{2\pi}{3})\frac{n\omega}{s^2+n^2\omega^2}+\sin(\varphi-\frac{2\pi}{3})\frac{s}{s^2+n^2\omega^2} \\ \cos(\varphi+\frac{2\pi}{3})\frac{n\omega}{s^2+n^2\omega^2}+\sin(\varphi+\frac{2\pi}{3})\frac{s}{s^2+n^2\omega^2} \end{pmatrix} \quad \text{(A4)}$$

Comparing to the Laplace transform of V_c, evaluated at $s=jn\omega$, it is deduced:

$$\begin{pmatrix} V'_{C1}(s) \\ V'_{C2}(s) \\ V'_{C3}(s) \end{pmatrix} = \frac{n\omega}{s} \begin{pmatrix} V_{C1}(s) \\ V_{C2}(s) \\ V_{C3}(s) \end{pmatrix} \quad \text{(A5)}$$

Substituting eq. (A5) back to eq. (A2) yields eq. (12).

VII. REFERENCES

[1] M. Prodanovic, T. C. Green. "Control and Filter Design of Three-Phase Inverters for High Power Quality Grid Connection", IEEE Trans. on Power Electronics, Vol. 18, No. 1, January 2003.

[2] T. Kawabata, T. Miyashita, Y. Yamamoto. "Dead Beat Control of Three Phase PWM Inverter", IEEE Trans. on Power Electronics, Vol. 5, No. 1, January 1990.

[3] E. Twining, D. G. Holmes. " Grid Current Regulation of a Three-Phase Voltage Source Inverter With an LCL Input Filter", IEEE Trans. on Power Electronics, Vol. 18, No. 3, May 2003.

[4] M. Lindgren, J. Svensson. "Control of a Voltage-source Converter Connected to the Grid through an LCL-filter - Application to Active Filtering", Proc. IEEE PESC 1998, pp.229-235.

[5] D. N. Zmood, D. G. Holmes, G. H. Bode. "Frequency-Domain Analysis of Three-Phase Linear Current Regulators", IEEE Trans. on Industry Applications, Vol. 37, No. 2, March/April 2001.

[6] IEC 61000-3-6:1996 Electromagnetic compatibility (EMC) -- Part 3: Limits - Section 6: Assessment of emission limits for distorting loads in MV and HV power systems. - Basic EMC publication.